**Supplementary Figure Legends**

**Supplementary Figure 1: Cross-tissue analysis of accessible chromatin with eGFRcrea-associated variants**

**a**) Fraction of overlap of 35,881 variants associated with eGFR across 29 tissues. 3,304 variants from 471 independent genetic signals overlap with accessible chromatin. **b**) Cumulative number of eGFRcrea-associated variants and signals overlapping accessible chromatin in the respective tissue. **c**) Number of variants per tissue that co-incide with chromatin uniquely accessible in the respective tissue

**Supplementary Figure 2: Cross-tissue analysis of the top 50,000 REs per tissue with PPA-filtered eGFRcrea variants**

**a**) Cumulative number of PPA-filtered eGFRcrea-associated variants and signals co-inciding with open chromatin in the top 50,000 REs for each tissue. **b**) Number of PPA-filtered variants in chromatin uniquely accessible in the top 50,000 REs in the respective tissue.

**Supplementary Figure 3: Refinement of eGFRcrea association signals at accessible chromatin by using additional kidney function biomarkers**

Cumulative number of genetic eGFR signals across accessible chromatin in the 29 tissues stratified according to their association with eGFRcrea alone (eGFRcrea only) or eGFRcrea with additional validation by cystatin C and/or blood urea nitrogen (eGFRcrea/eGFRcys and/or BUN validated).

**Supplementary Figure 4: Proportion of eGFR variants in accessible chromatin of the kidney or PTC according to PPA value.**

**a**) and **b**) Proportion of RE-positive variants against the PPA level in a) PTC or b) kidney according to their association with eGFRcrea alone (eGFRrea only) (light blue dots) or eGFRcrea with additional validation by cystatin C and/or blood urea nitrogen (eGFRcrea/eGFRcys and/or BUN) (dark blue triangle). rs77924615 has a PPA of 100% (two variants with 100% in the set) and overlaps accessible chromatin in both samples (PTC and kidney).

**Supplementary Figure 5: Activity-by-contact (ABC) model predicts enhancer-promoter interactions at eGFR associated loci**

**a**) and **b**) Genomic locus of the *TCEA2* and *RGS19* genes. Indicated are eGFRcrea variants, eQTL variants (tub/int, tubulointerstitial compartment of the kidney from Hu et al.), H3K27ac ChIP-seq as well as ATAC-seq from PTC derived from the same individual (donor 2 in a) and donor 3 in b)). The ABC model suggests interactions of the variant-carrying RE with both promoters (dark magenta). The SNPs rs6062343 and rs6062344 are eQTLs for *RGS19* in the tubulo-interstitial compartment of the kidney.

**Supplementary Figure 6: HNF-1β CUT &Tag-seq and HNF-1β binding at rs77924615 within the *UMOD/PDILT* locus**

**a)** Venn plot depicting overlap of HNF-1β binding sites between the five different PTC HNF-1β CUT&Tag-seq experiments. **b)** HNF-1β CUT&Tag-seq tracks at the *UMOD/PDILT* gene locus generated from PTC from five individual donors (a-e). ATAC-seq from one PTC experiment and HNF-1β ChIP-seq from one PTC experiment are shown for comparison. eGFRcrea and eQTL variants are indicated (tub/int, tubulointerstitial compartment of the kidney from Hu et al.). rs77924615 is an eQTL for *UMOD* in the tubule-interstitial compartment as defined by Han et al. **c)** Bar plot depicting the percent of variant-carrying and HNF-1β-associated REs from PTC co-incided with accessible chromatin across the 29 tissues. Overlap of REs with variants containing HNF-1β motifs (dark blue) or containing HNF-1β motifs and intersecting HNF-1β binding (light blue) are shown across the 29 tissues.

**Supplementary Figure 7: HNF-1β binding at a polymorphic RE next to the *NDRG1* promoter**

**a**) and **b**) Sequencing tracks from HNF-1β and H3K27ac CUT&Tag-seq as well as ATAC-seq performed in PTC (donor 2 in a) and donor 3 in b)) at the rs10283362-*NDRG1* locus. Activity-by-contact (ABC) analysis was used to predict promoter-enhancer interactions. eGFRcrea associated and eQTL variants (tub/int, tubulointerstitial compartment of the kidney from Hu et al.) are indicated.

**Supplementary Figure 8: HNF-1β binding at the *NDRG1* enhancer**

**a**) HNF-1β CUT&Tag-seq tracks at the *NDRG1* gene locus generated from PTC from five individual donors. ATAC-seq from one PTC experiment and HNF-1β ChIP-seq from one PTC experiment are shown for comparison. **b**) ATAC-seq from one PTC experiment and single nucleus ATAC-seq (snATAC-seq) data in different compartments of the kidney (Muto, Y. et al. Nat Commun 12, 2190; 2021). Proximal convoluted tubules (PCT) are accessible at the *NDRG1* enhancer containing rs10283362.

**Supplementary Figure 9: rs10283362-associated enhancer regulates *NDRG1* gene expression in PTC**

**a**) Schematic of the *NDRG1* locus, the candidate cis-regulatory element (cCRE) with variant rs10283362 and the position of the single guide RNA (sgRNA) used for CRISPR/Cas9 experiments. **b**) NDRG1 mRNA expression in PTC after CRISPR/Cas9-mediated knock-out of the rs10283362 carrying sequence (KO) compared to non-targeting sgRNA transfected cells (Ctrl.). Data was from six independent donors, was normalized on values from one sample from Ctrl.1, and is shown in mean +/- SD. Ordinary one-way ANOVA for multiple comparisons was performed; **, $p<0.01$. **c**) NDRG1 protein expression in control and *NDRG1* enhancer knock-out cells from a representative experiment.

**Supplementary Figure 10: Sanger sequencing of HK-2 *NDRG1* enhancer knock-out cells**

**a**) and **b**) Sanger sequencing tracks from HK-2 Ctrl. vs. KO cells of clones (KO1 in a) and KO2 in b)) were analyzed using Sanger sequencing to identify mutations. The sgRNA binding site is highlight as a black line in the control sequence.

**Supplementary Figure 11: Knock-out of the rs10283362 carrying sequence in the *NDRG1* enhancer leads to reduced HNF-1β binding and enhancer activity at this locus**

HNF-1β and H3K27ac CUT&Tag-seq tracks from HK-2 ctrl. (Ctrl. 1, blue) and *NDRG1* enhancer KO cells (KO 1, turquoise). Shown are the *NDRG1* promoter, the *NDRG1* enhancer (red box) and the HNF-1β binding control locus *FXYD2*.

**Supplementary Figure 12: *NDRG1* enhancer knock-out clone 2 reveals a defective migration behavior**

**a**) Representative pictures of HK-2 Ctrl. 2 vs. *NDRG1* enhancer KO clone 2 from the wound healing assay at the timepoints 0 and 12 hours. **b**) Cell tracking analysis from wound healing assay of 60 individual cells of clones (Ctrl. 2 and KO 2) shows the route migrated by each cell over a duration of 12 hours.

**Supplementary Figure 13: Knock-out of exon 2 of the *NDRG1* gene shows comparable effects to *NDRG1* enhancer knock-out clones of cells**

**a**) Schematic of the *NDRG1* locus with the first two exons, the candidate cis-regulatory element (cCRE) (green) with variant rs10283362 (red) and the position of the single guide RNA (sgRNA) in exon 2 used for CRISPR/Cas9 experiments. **b**) NDRG1 protein expression in the two control clones and the *NDRG1* exon knock-out clone of HK-2 cells (*NDRG1* exKO) reveals knock-out of the protein. **c**) Sanger sequencing tracks from HK-2 Ctrl. vs. *NDRG1* exKO clones of cell to verify the knock-out results. The sgRNA binding site is highlight as a black line in control sequence. **d**) Volcano plot from RNA-seq experiments in HK-2 *NDRG1* exon knock out vs. intact enhancer control clones of cells. **e**) GO Hallmark analysis of down- or upregulated genes from the RNA-seq experiment (*NDRG1* exKO vs Ctrl.) using Metascape platform. DEGs were based on adjusted p-value < 0.05 and $\log_2$(fold change) ≥ $\log_2$(0.5) or ≤ $\log_2$(-0.5). **f**) Proliferation assay of control (blue) and *NDRG1* exKO (purple) clones of cells using an MTS assay (n=6; with three replicates each). Multiple, unpaired t-test was performed; *, p< 0.05; **, p<0.01. **g**) Wound healing assay of control and *NDRG1* exKO cells of clone imaged in a live cell imaging experiment. Depicted is the percentage of closure of the gap over time [h]. Data (n=8) shown in mean +/- SD. Two-way ANOVA for multiple comparisons was performed; *, p< 0.05; ***, p< 0.001; p< ****, p<0.0001. **h**) Representative pictures of control vs. *NDRG1* exon KO cells of clone from the wound healing assay at the timepoints 0 and 12 hours. **i**) Cell tracking from wound healing assay of 60 individual cells (Ctrl. 1 and *NDRG1* exKO) shows the route migrated by each cell over a duration of 12 hours. **j**) Accumulated distance [µm] for each of the 60 cells (Ctrl. 1, Ctrl.2, *NDRG1* exKO) over 12 hours. **k**) Corresponding Euclidean distance [µm] of the Ctrl. and *NDRG1* exKO cells. **l**) Velocity [µm/min] for Ctrl. 1, Ctrl.2, *NDRG1* exKO cells in the migration assay. **m**) Directional migration of the cells (Ctrl. and

*NDRG1* exKO). Whereby a value of 1 represents a linear movement, a value less than 1 indicates an undirected migration. Data shown in mean +/- SD. Ordinary one-way ANOVA for multiple comparisons was performed; *, p< 0.05; ***, p< 0.001; p< ****, p<0.0001.

# Supplementary Figure 1

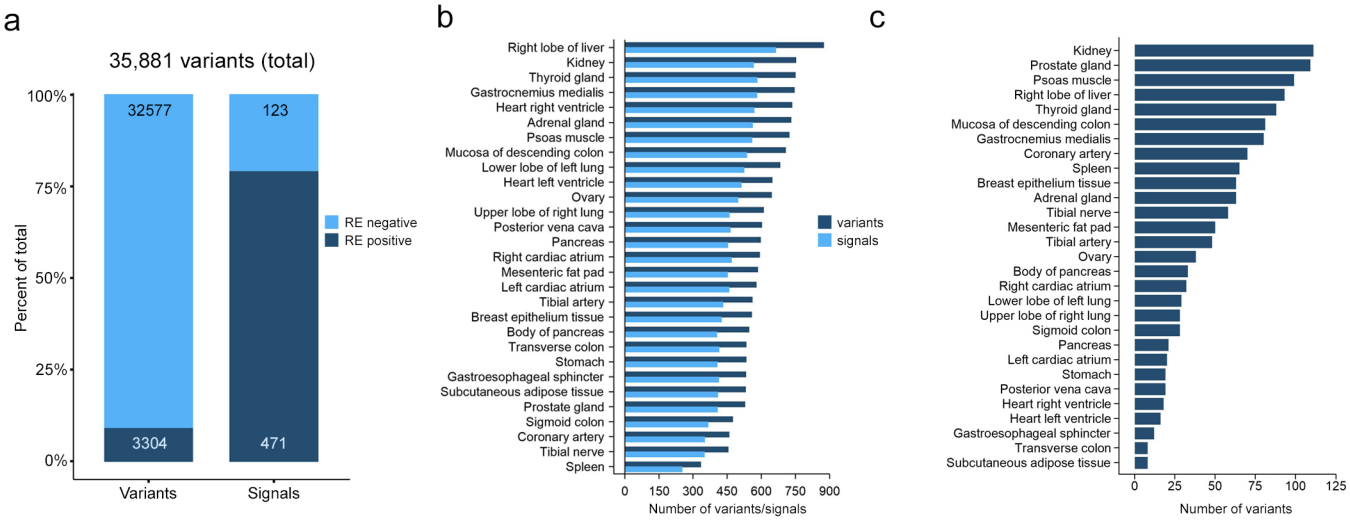

# Supplementary Figure 2

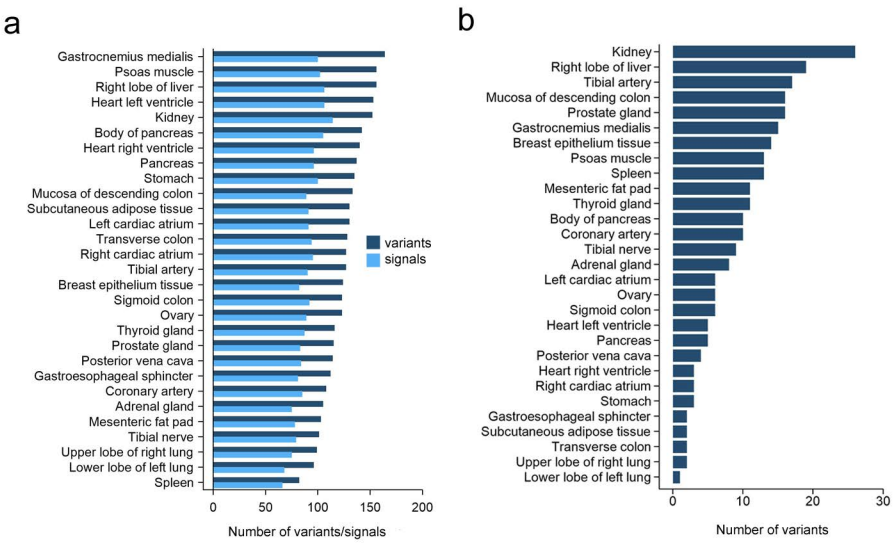

# Supplementary Figure 3

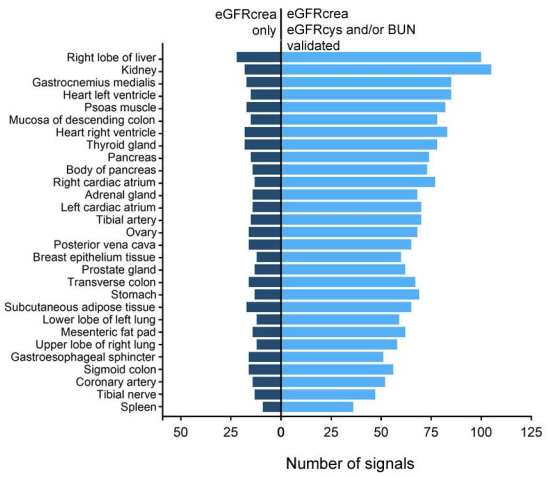

Supplementary Figure 4

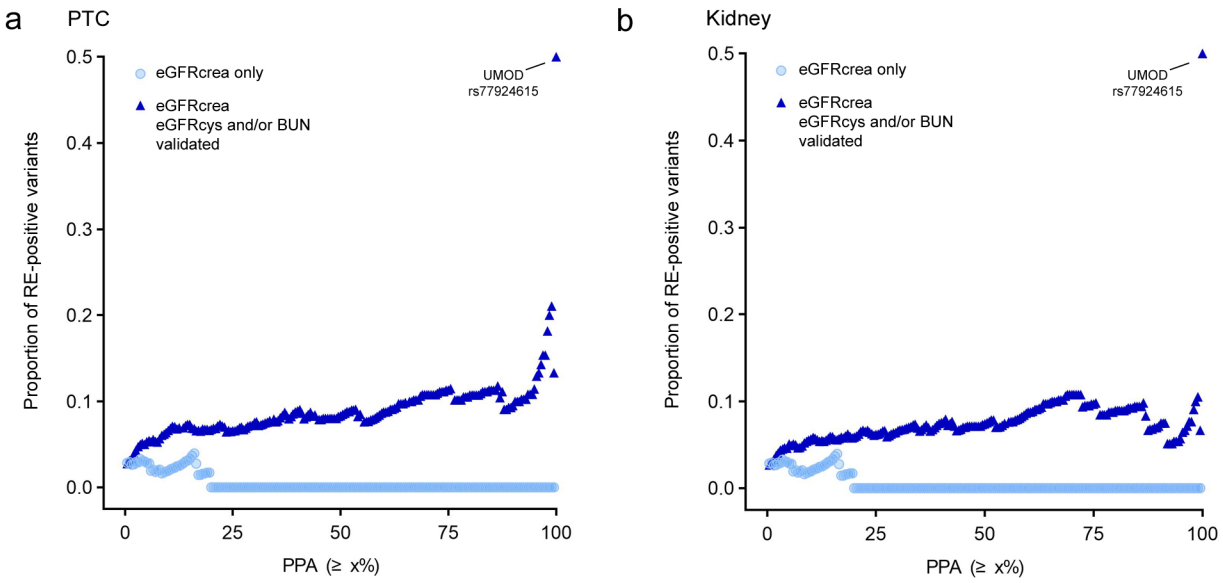

# Supplementary Figure 5

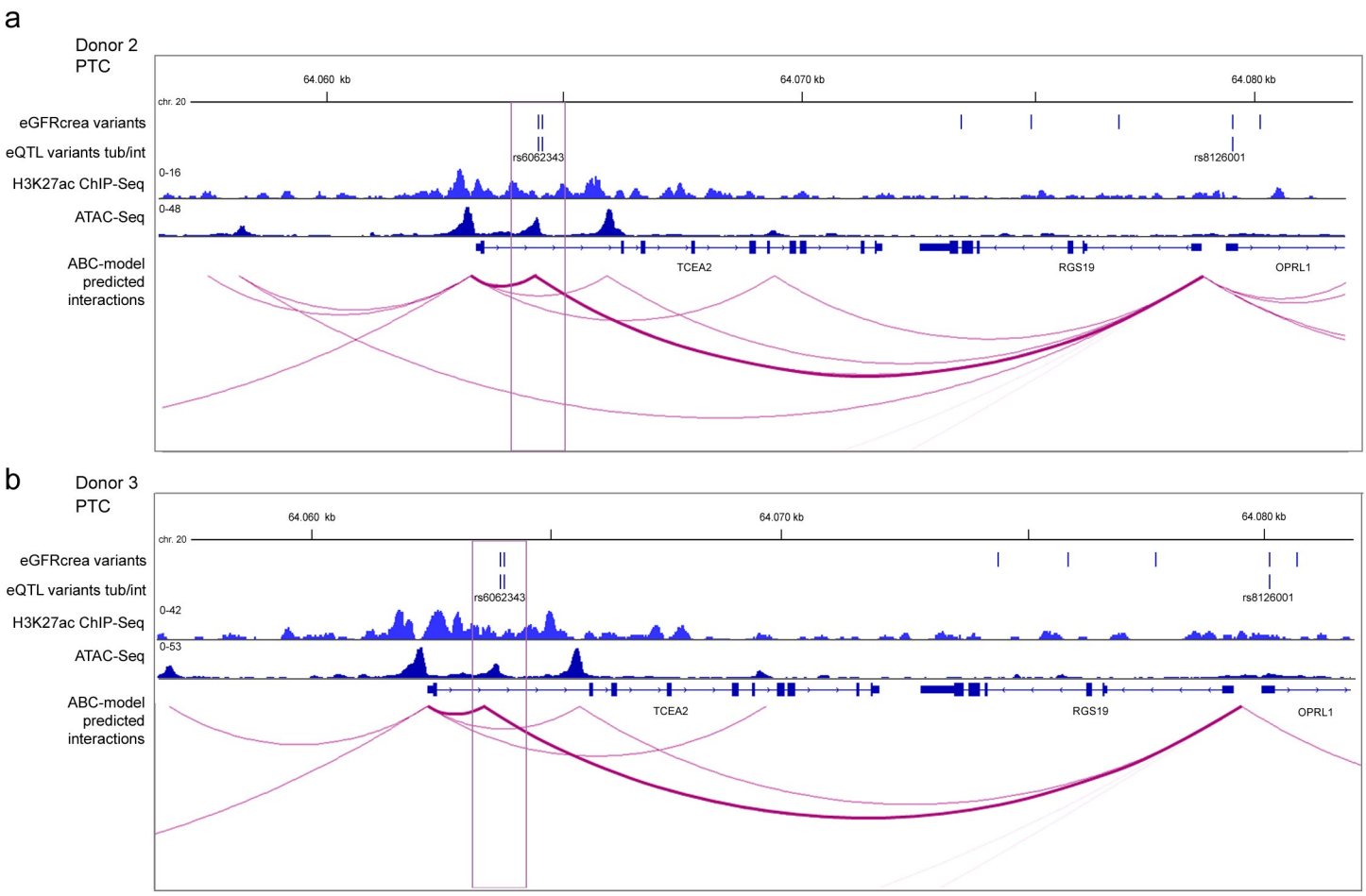

# Supplementary Figure 6

a

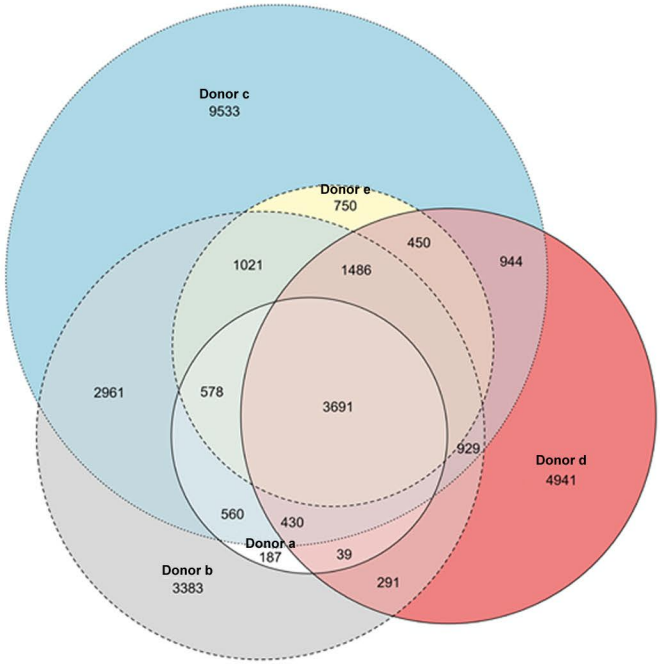


b

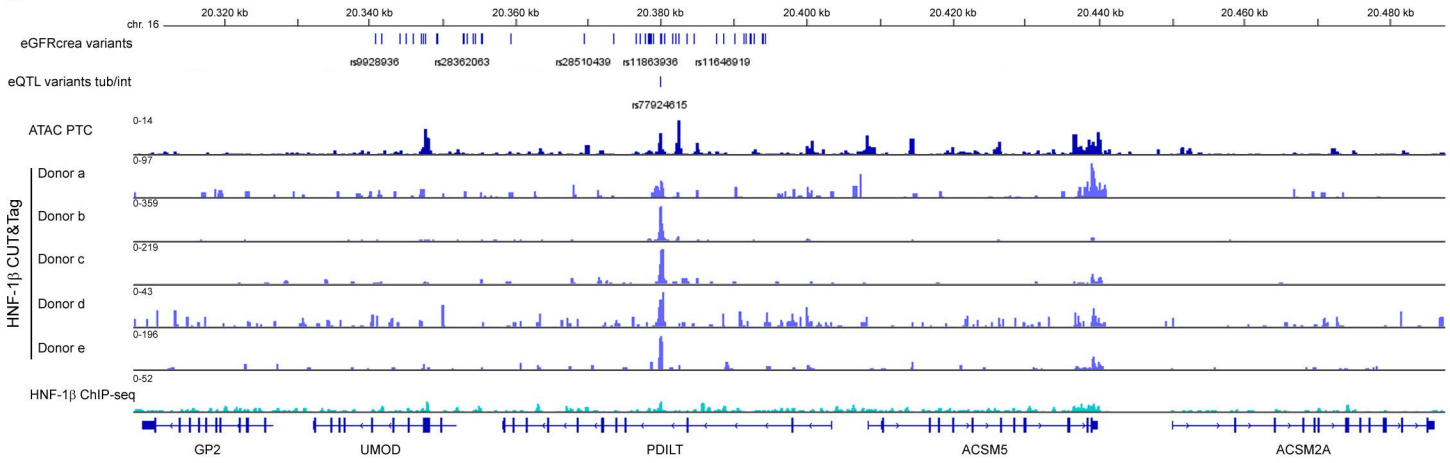


c

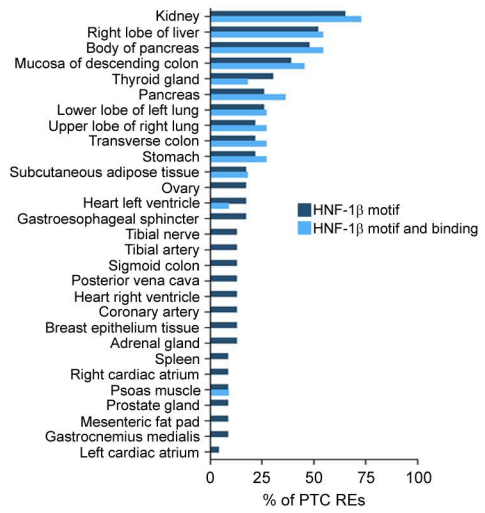

Supplementary Figure 7

a

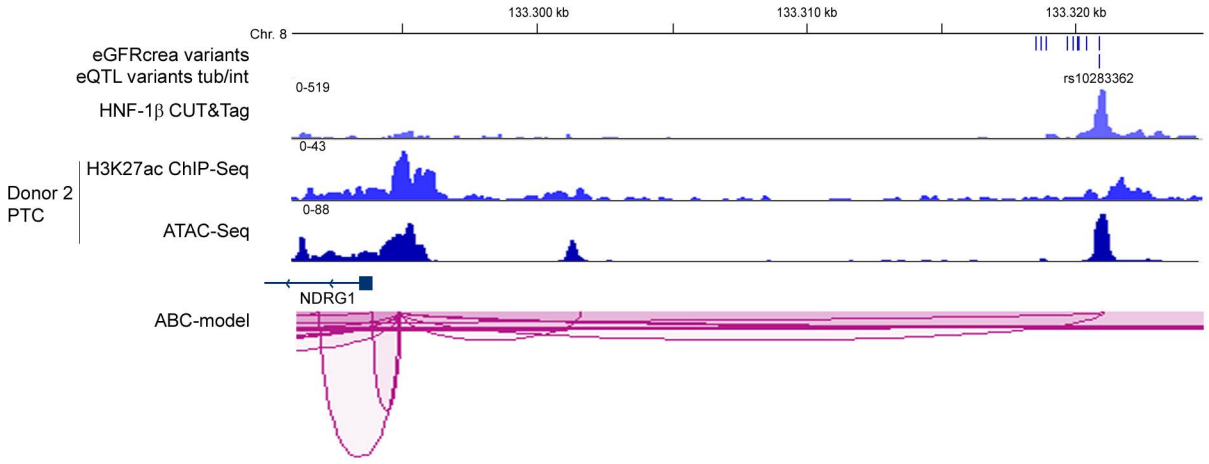


b

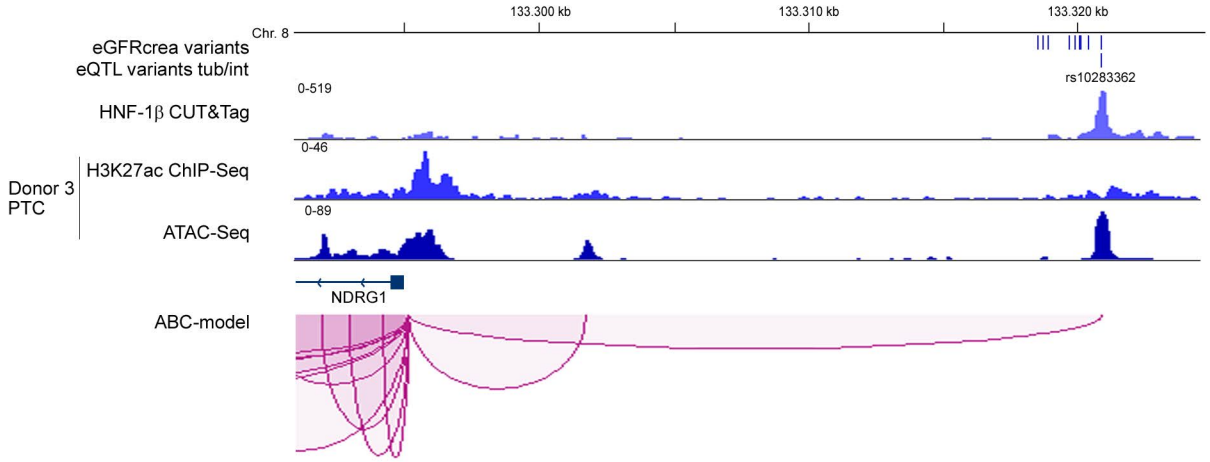

# Supplementary Figure 8

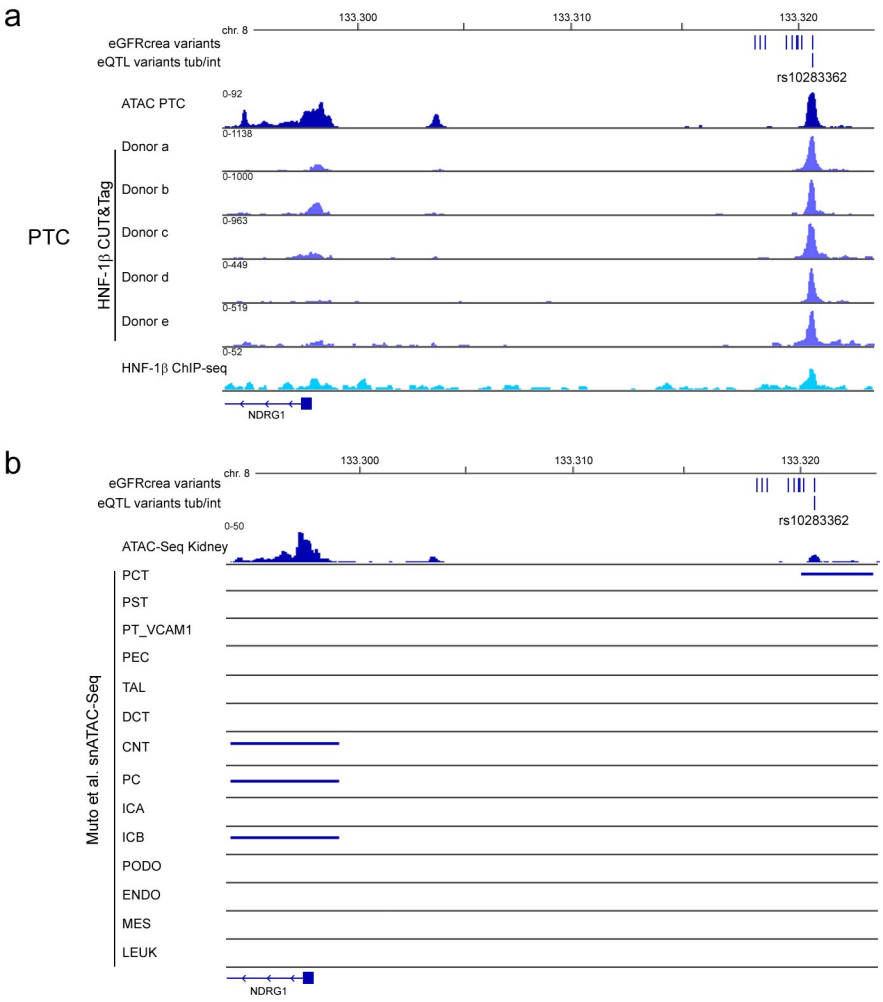

Supplementary Figure 9

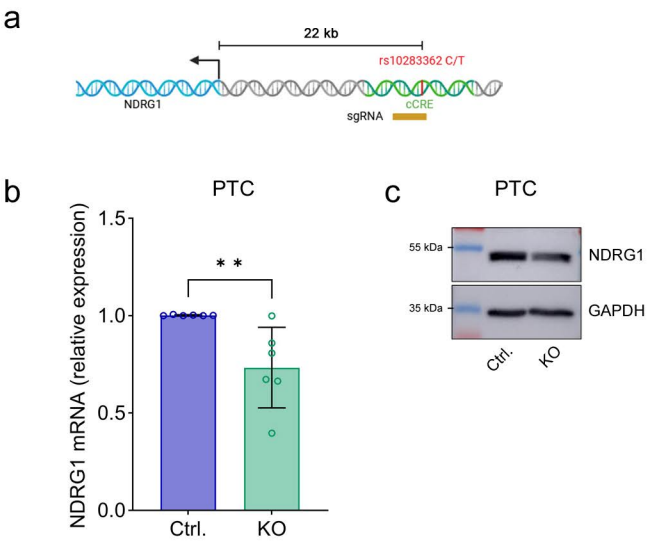

Supplementary Figure 10

a HK-2 KO 1 vs. Ctrl.

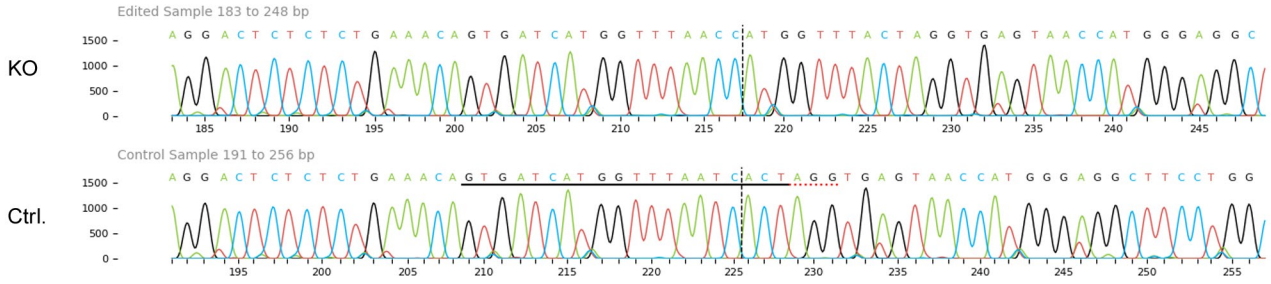


b HK-2 KO 2 vs. Ctrl.

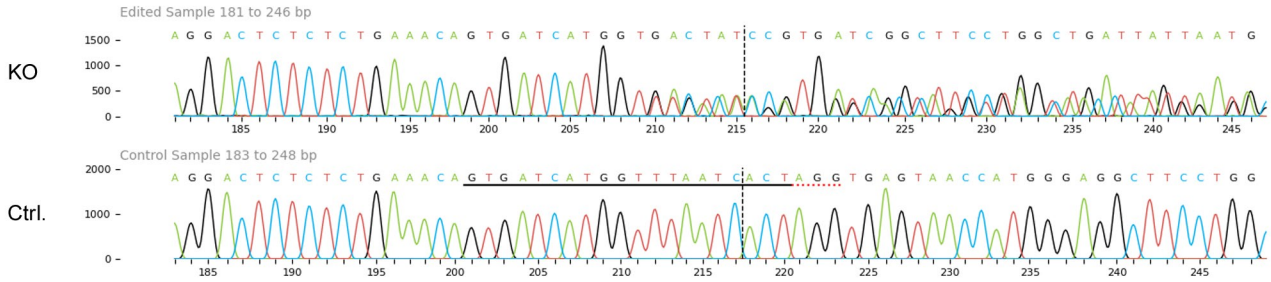

# Supplementary Figure 11

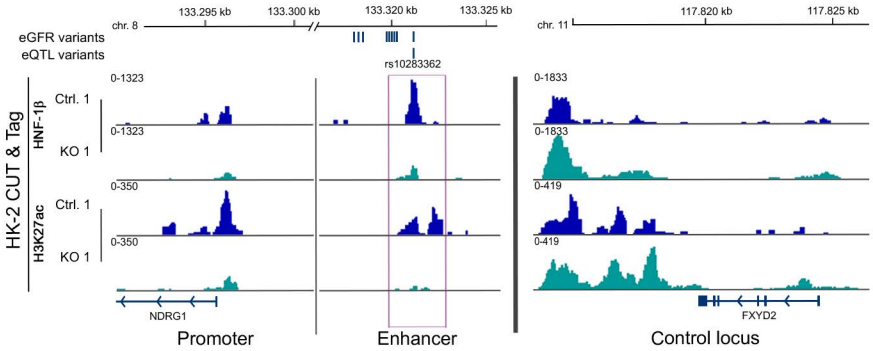

Supplementary Figure 12

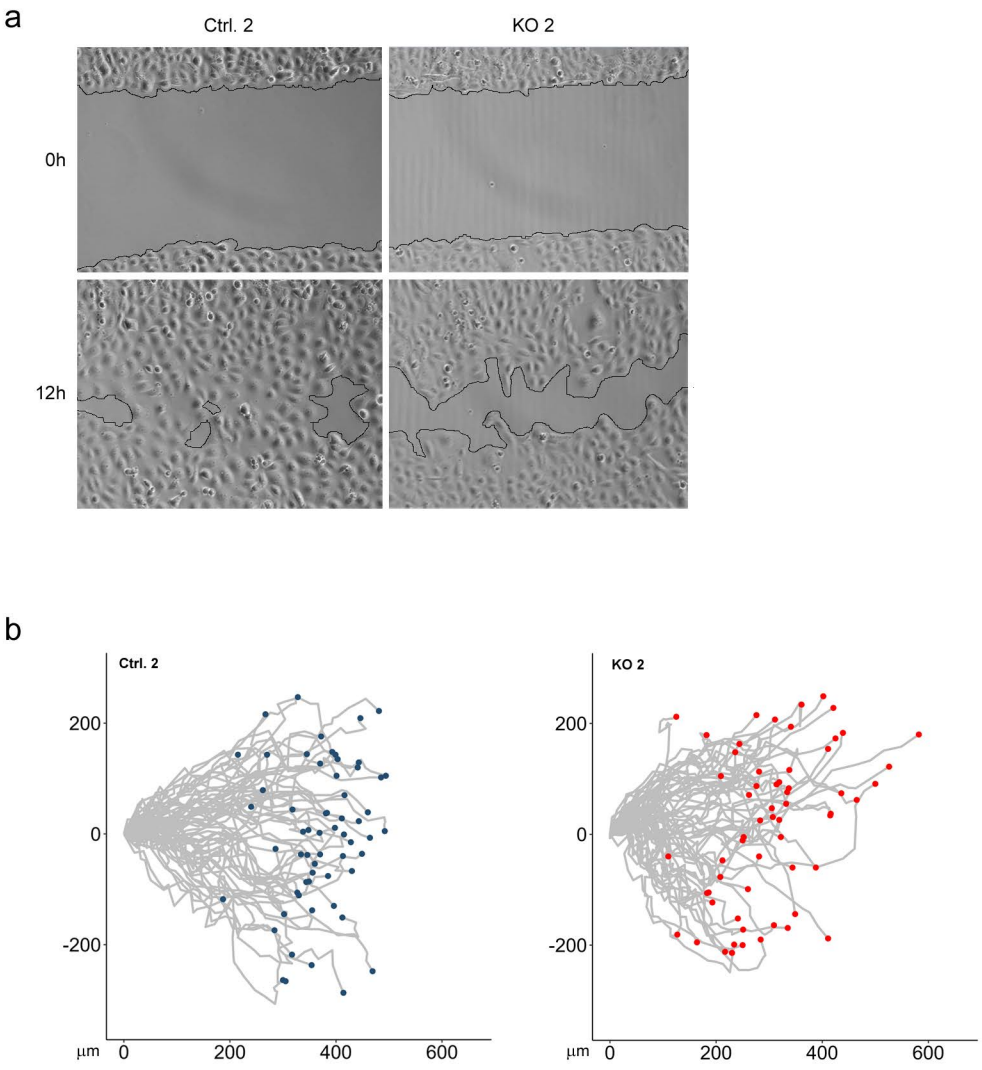

# Supplementary Figure 13